Science Advances

AAAS

advances.sciencemag.org/cgi/content/full/4/3/eaar2982/DC1

Supplementary Materials for

Fluid pressure and shear zone development over the locked to slow slip region in Cascadia

Pascal Audet and Andrew J. Schaeffer

Published 7 March 2018, *Sci. Adv.* **4**, eaar2982 (2018)
DOI: 10.1126/sciadv.aar2982

This PDF file includes:

Supplementary Text

section S1. Seismic velocity models.

We consider a suite of models that aim to reproduce the main characteristics of the observed CCP image: 1) a dipping low-velocity layer (LVL); 2) apparent disappearance of the LVL at depth <20 km and flattening of the bottom LVL boundary; 3) increased negative amplitude near but down dip of the low-frequency earthquake cluster; and 4) flattening of the top boundary of the LVL at the down dip end of the profile. We proceed by generating seismic velocity models based on two slab depth models (RF slab model (*12*) and USGS slab model (*20*)) interpolated along the linear profile, and using uniform background seismic velocities from published work in this area (*13*) (table S1), unless specified otherwise. We construct eight different seismic velocity models with the aim to incrementally improve the cross-correlation and misfit values (i.e., increase the RIF). The first four models aim to produce a reference model by testing the Vp/Vs value for the LVL as well as its position above or below the plate interface using both slab models. The remaining four models are refinements of the resulting reference model. These models are defined below.

Model 1: A 3-km thick LVL with v_p/v_s of 1.78 located below the plate interface;
Model 2: A 3-km thick LVL with v_p/v_s of 1.78 located above the plate interface;
Model 3: A 3-km thick LVL with v_p/v_s of 2.0 located below the plate interface;
Model 4: A 3-km thick LVL with v_p/v_s of 2.0 located above the plate interface;
Model 5: An LVL with v_p/v_s of 2.0 and thickness that linearly increases from 1 to 2 km offshore and from 2 to 6 km onshore, located above the plate interface;
Model 6: Same as Model 5 with a locally increased v_p/v_s of 3.5 immediately down dip of the low-frequency earthquakes and a wedge-shaped LVL with a top boundary flattening at a depth of 32 km (RF model) or 40 km (USGS model);
Model 7: Same as Model 6 with progressively reduced seismic velocities in the overlying fore arc crust offshore;
Model 8: Same as Model 7 but for which the layer offshore has average oceanic crust velocities (effectively a 0-km LVL offshore).

The velocity models, synthetic receiver functions and the resulting images are shown in fig. S4. We note that the low-velocity signature above depths of ~15 km disappears for all models considered, even if we used a higher frequency corner (up to 1 Hz). This results from the combination of the shallow depth and small layer thickness, essentially suppressing the time delay between the forward and back-scattered phases and producing incoherent stacks. The CC and the MM values for each slab depth model (RF and USGS) and seismic velocity model (1 to 8) are shown in fig. S5. We first note that for all seismic velocity models examined (Models 1 to 8), the ones that use RF slab model produce higher cross-correlation and lower misfit values than those based on the USGS slab model.

Consider first the results for Models 1 to 4. Regardless of the v_p/v_s values of the LVL, placing it above the slab interface improves both the CC (~3-7%) and MM values (-1%) (Models 2 vs 1; Models 4 vs 3). Increasing the v_p/v_s of the LVL from 1.78 to 2.0 increases the MM (~1%) for both slab models (Models 3 vs 1; Models 4 vs 2); the increase in MM is lowest when the RF slab

model is used and the LVL is placed above the slab (~0.4%). However, in this case the increase in CC values is much higher (~15-20%) than the increase in MM (~1%), regardless of the slab depth model used (Models 3 vs 1; Models 4 vs 2). For these first four seismic velocity models, the highest RIF is obtained for the RF slab model between Models 4 and 1 (25%); Model 4 with the RF slab model also has the highest cross-correlation value. Based on these results, we select Model 4 as the reference model and proceed to test further refinements of the model.

Model 5 aims to examine a down dip increase in LVL thickness, as surmised in previous work (*13*, *21*, *22*). Selecting the RF slab model and seismic velocity Model 4 as reference, the RIF is 7% with CC value increasing by 7% with negligible MM reduction (-0.1%). Model 6 further examines a locally increased v_p/v_s near the tremor source region (from 2.0 to 3.5), as well as a flattening of the top LVL boundary observed toward the easternmost part of the profile. The flattening effect is modeled as a wedge of LVL (v_p/v_s of 2.0) with a flat top boundary at ~32 km depth for the RF slab model, and ~40 km for the USGS slab model (i.e., at the same horizontal position along the profile). Taking RF slab model and seismic velocity Model 5 as reference, the RIF is 16%, most of it explained by a corresponding increase in CC value (MM change of -0.5%). Note that the USGS slab model shows a RIF of -17%, significantly deteriorating the fit from Model 5 to 6, likely because the two slab models are most different in the down dip portion of the profile.

Model 7 aims to examine the effect of lower seismic velocities in the offshore portion of the overlying fore arc, due to sediment accumulation. This is modeled as a progressive decrease in bulk seismic velocities trench-ward. Because the changes in seismic velocity models all occur offshore where the corresponding structure in the images is more subdued, we expect much more modest improvements in cross-correlation values. Selecting the RF slab model and seismic velocity Model 6 as reference, the RIF is 4%. Finally, we test a final model (Model 8) by increasing seismic velocities and v_p/v_s of the low-velocity layer to those of average oceanic crust in the offshore portion. Selecting the RF slab model and seismic velocity model 7 as reference, the RIF is small at 0.7%, all of it due to a reduction in MM. Even though the improvement is very modest, using hypothesis testing this result implies that addition of a low-velocity layer with high v_p/v_s in the offshore region (Model 7) increases the misfit and is therefore not statistically required by the receiver function data.

Although our models are not unique, the incremental construction of the seismic velocity models following a positive trend in relative improvement factors provides quantitative evidence that receiver function data are characterized by a low-velocity layer with high v_p/v_s (~2.0) but only at depth >15 km, and whose thickness increases from ~2 to 6 km down dip to a depth of >30 km. The data also require significantly increased v_p/v_s values near the tremor source region as well as a flattening of the top boundary near 32 km depth, potentially reflecting the intersection with the mantle wedge corner.

Supplementary Figures

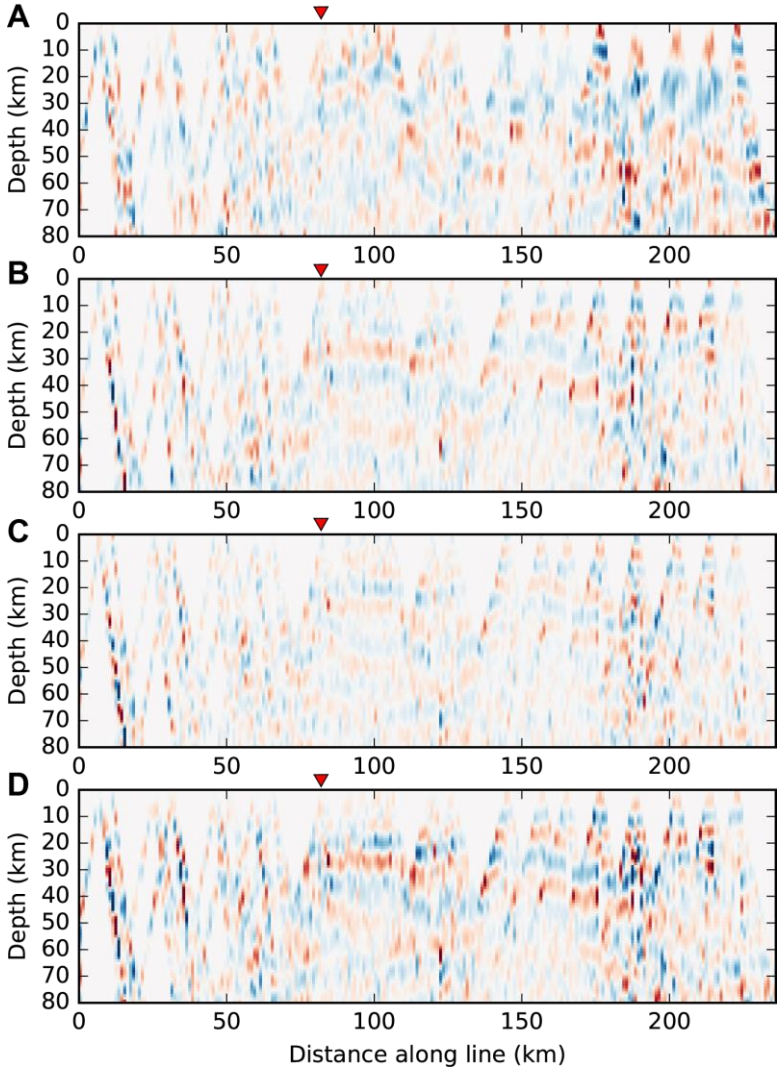

fig. S1. CCP images. A, Forward-converted Ps and back-scattered Pps (**B**) and Pss (**C**) phases. **D**, Weighted sum of **A**-**C** where the Pps and Pss stacks have 3 times the weight of the Ps stack.

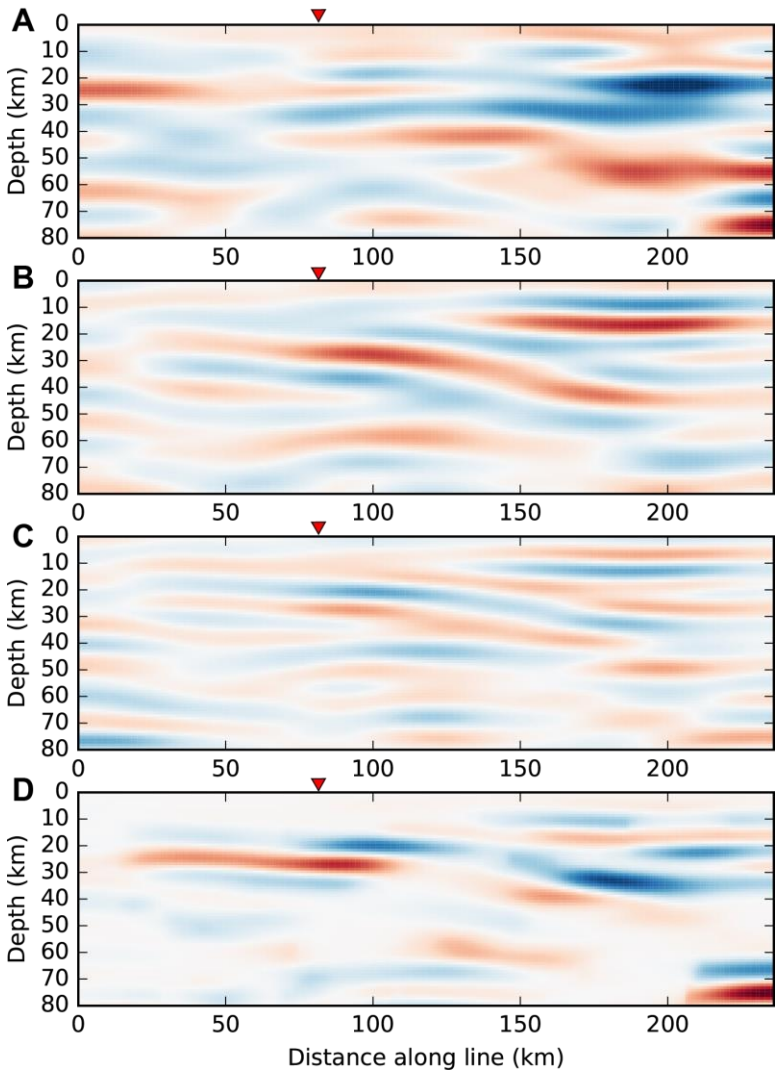

fig. S2. Gaussian-weighted CCP images. A, Forward-converted Ps and back-scattered Pps (**B**) and Pss (**C**) phases. **D**, Phase-weighted sum of **A**-**C** that suppresses incoherent signal between the three images and eliminates contamination by mis-mapped phases in each phase stack.

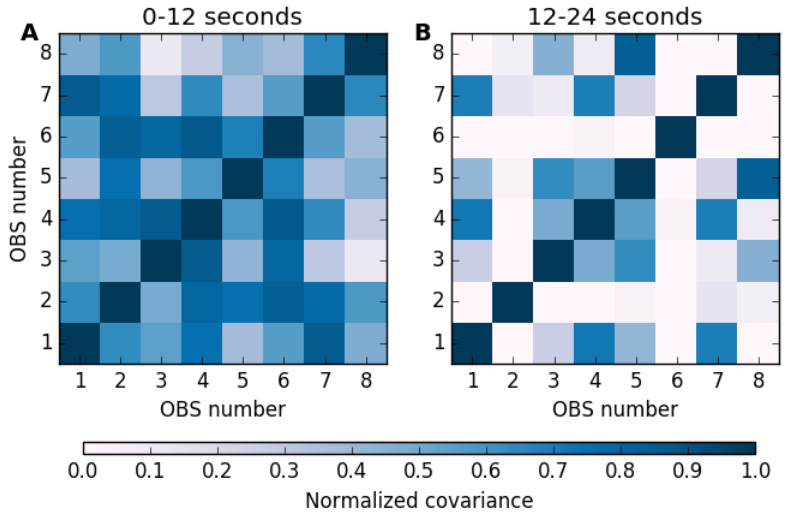

fig. S3. Normalized covariance values of receiver functions across the OBS stations used in the analysis. (**A**) Values obtained from the first 0 to 12 seconds and (**B**) between 12 to 24 seconds, showing the higher coherence of the OBS in the early part of the waveforms. The mean of the off-diagonal terms is 0.6 and 0.15 for **A** and **B**, respectively. OBS numbers from 1 to 8 correspond to stations FN12C, FN11C, FN08C, FN07C, FN04C, FN03C, FN02C, and FN01C, respectively.

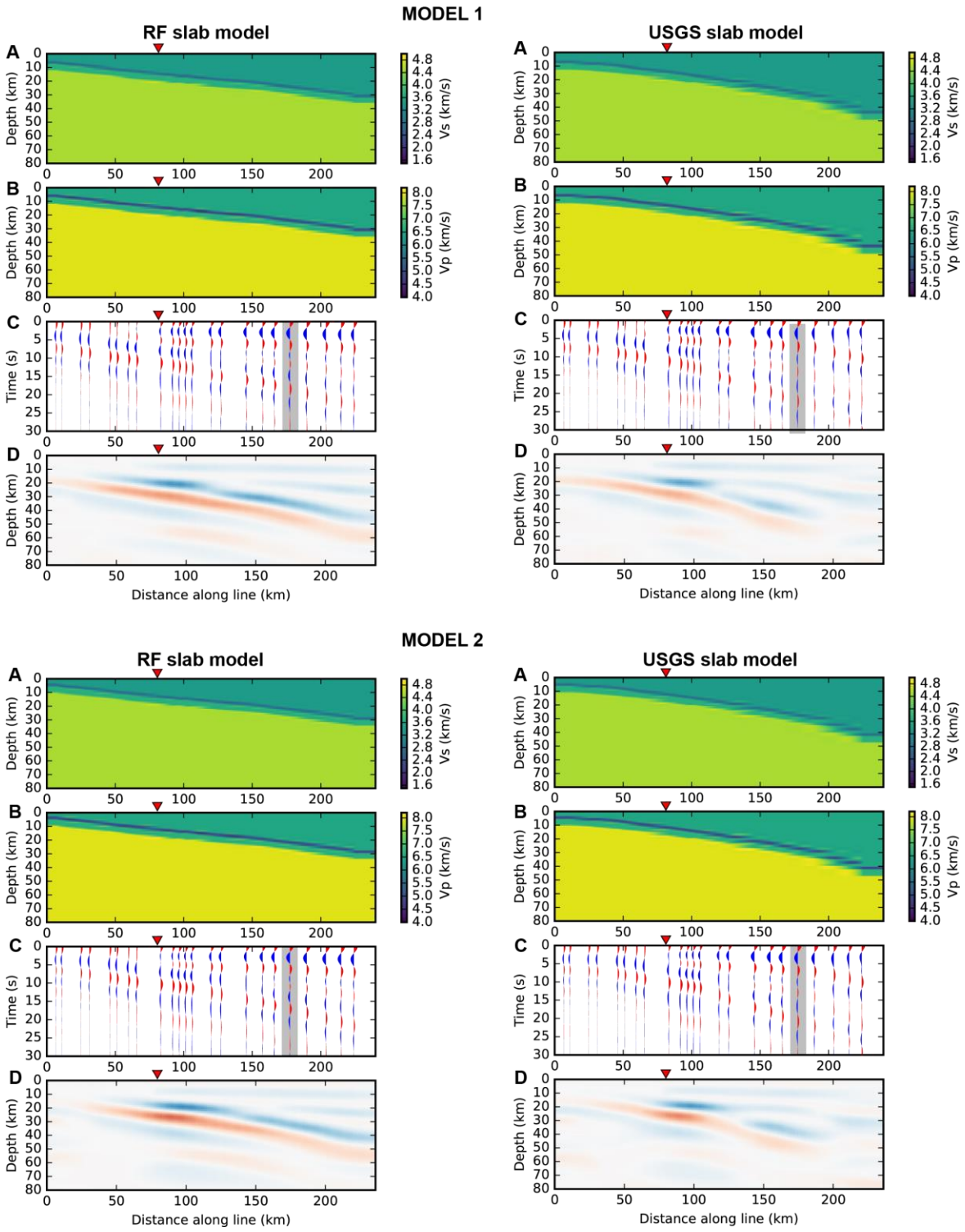

fig. S4. Synthetic models and results. A, **B**, Seismic velocity models resulting synthetic receiver functions (**C**) and Gaussian-weighted, phase-weighted CCP image (**D**) for Models 1 to 8 and using the RF slab model or USGS slab model. Grey shaded area in panels **C** correspond to stacked synthetic receiver functions calculated for station S050 (Fig. 2C).

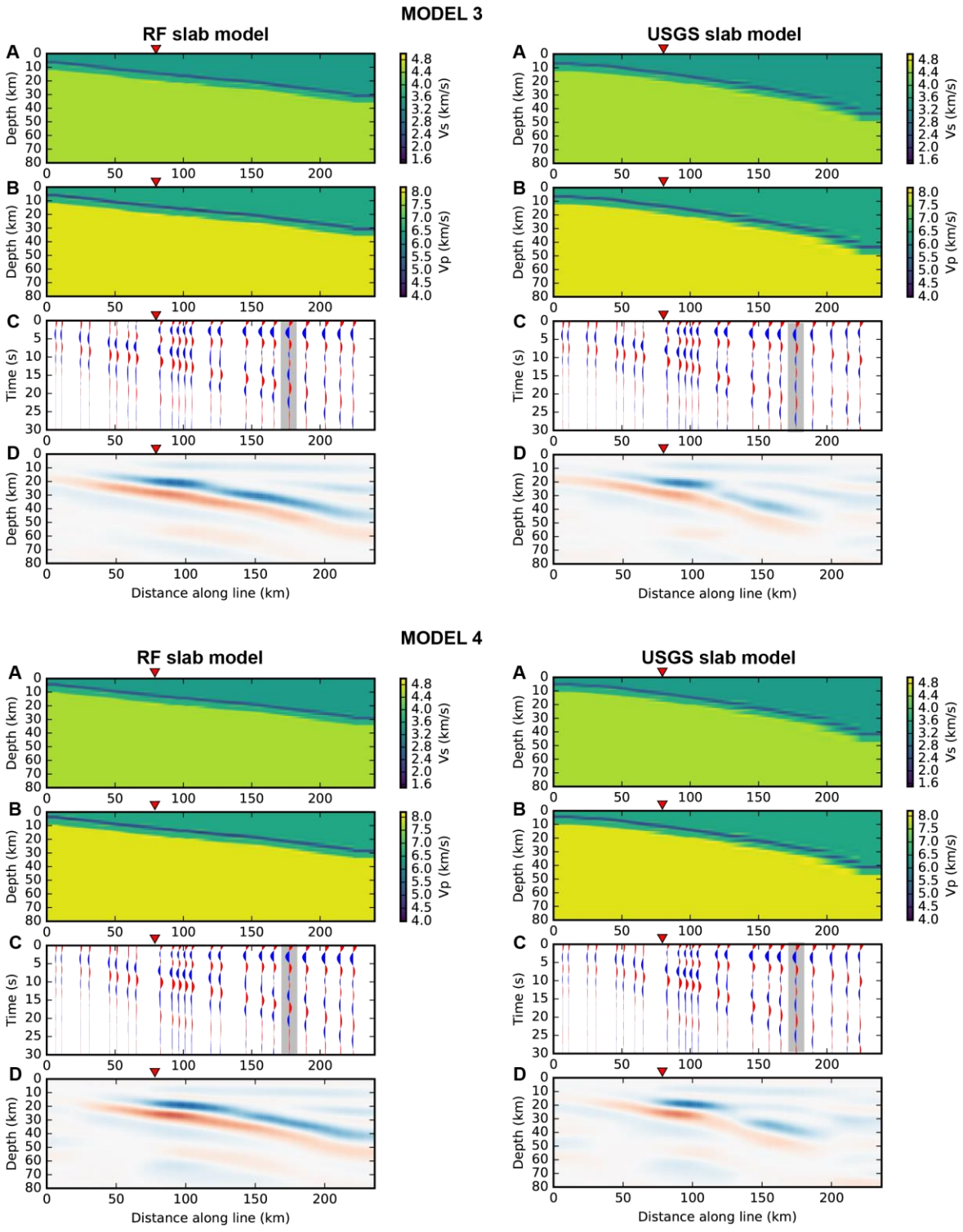

fig. S4. (continued)

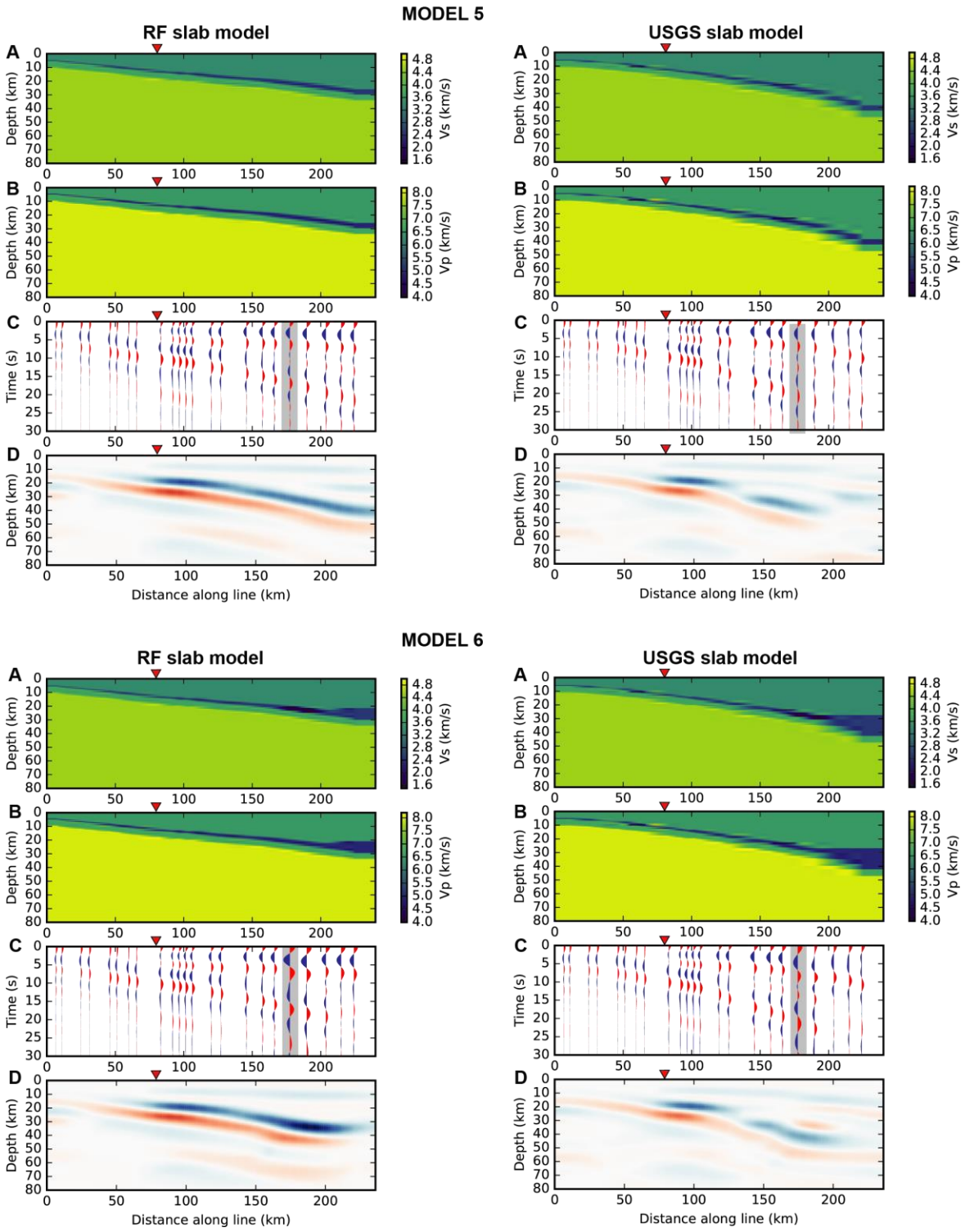

fig. S4. (continued)

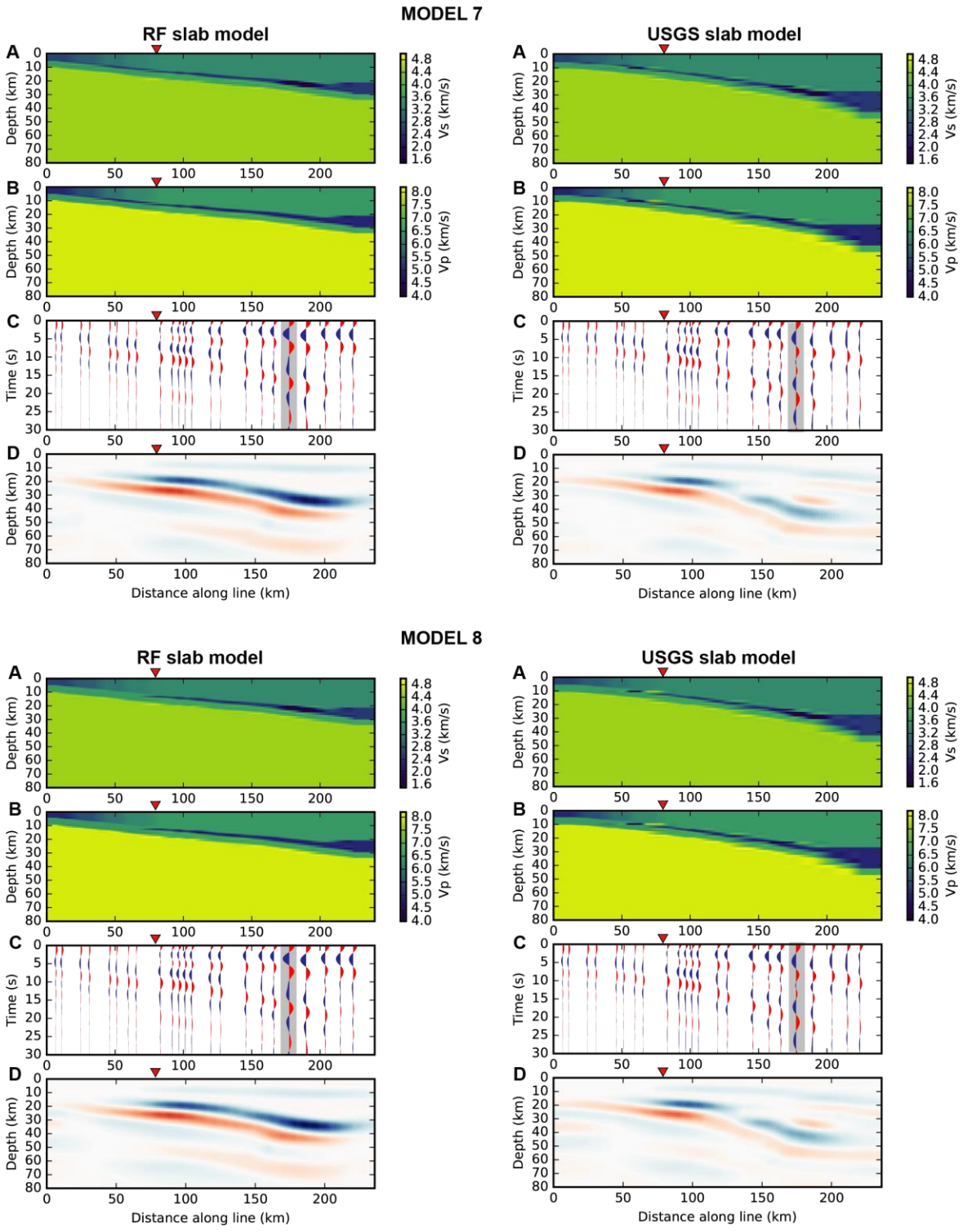

fig. S4. (continued)

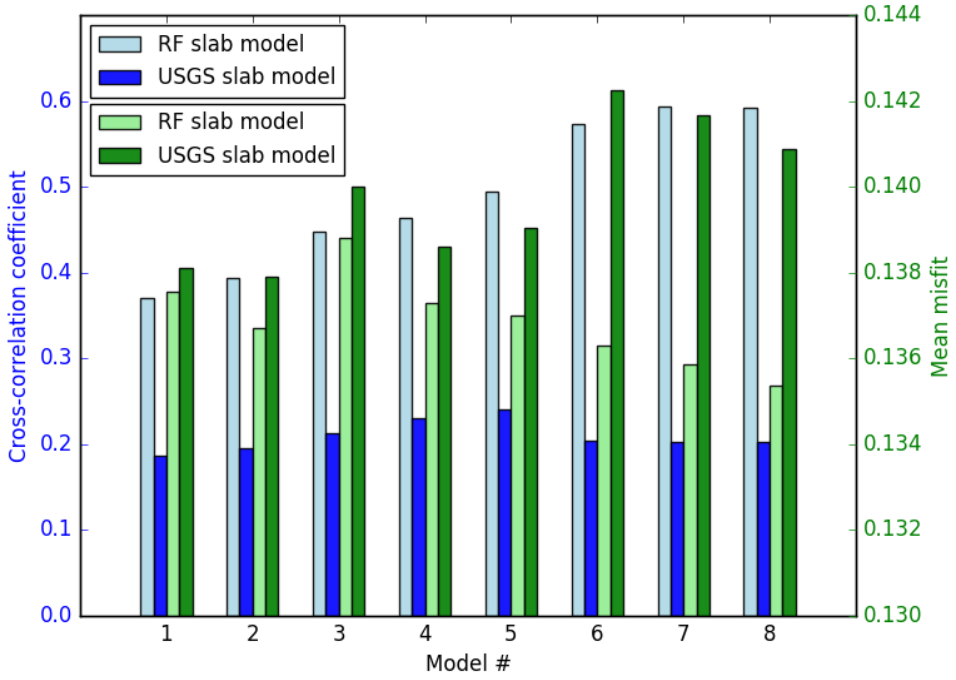

fig. S5. Quantitative comparison between observed and synthetic receiver function data and CCP images. Light and Dark colored bars show results for the RF slab model and the USGS slab model, respectively, for all seismic velocity models considered. Cross-correlation values are in blue; mean misfit values are in green.

Supplementary Table

table S1. Background seismic velocity model.

Layer	Thickness (km)	Density (kg/m3)	P-wave velocity (km/s)	S-wave velocity (km/s)
Fore arc crust	Variable	2800	6.5	3.4
Low-velocity layer	Variable	2800	5.0	Variable
Oceanic crust	6.5	2800	6.7	3.7
Upper mantle	Half-space	3200	8.0	4.6